Soft Matter

PAPER

View Article Online
View Journal

Cite this: DOI: 10.1039/d6sm00317f

Liquid crystalline order delays crystallisation in mixed surfactant systems

Sepideh Khodaparast, *[a] William N. Sharratt, [b] Robert M. Dalgliesh[c] and João T. Cabral [d]

Crystallisation in mixed surfactant systems is often preceded by the formation of intermediate self-assembled structures, whose influence on crystallisation pathways remains poorly understood. In particular, the emergence of liquid crystalline phases can impact both the onset and progression of crystallisation. Here, we investigate crystallisation upon cooling in aqueous mixtures of sodium dodecyl sulfate (SDS) and dimethyldodecylamine oxide (DDAO) at concentrations relevant to formulated systems, employing dynamic light scattering, cross-polarised optical microscopy, and small-angle neutron scattering. We find that addition of DDAO to 20% SDS promotes the formation of a hexagonal liquid crystalline phase, accompanied by a marked increase in viscosity and a pronounced change in crystallisation kinetics. While the apparent crystallisation temperature is only weakly affected beyond 3 wt% DDAO, the induction time for crystallisation increases by orders of magnitude for DDAO concentrations 5 wt%, indicating a strong retardation of crystallisation within the liquid crystalline regime. Time-resolved small-angle neutron scattering (SANS) reveals that crystallisation proceeds *via* a delayed transformation of the hexagonal phase, with coexistence of liquid crystalline and crystalline structures over extended timescales. This kinetically hindered pathway associated to liquid crystalline order can be exploited to postpone crystallisation (and thus increase metastability) in surfactant formulations without significant changes to overall composition.

Received 10th April 2026,
Accepted 7th May 2026

DOI: 10.1039/d6sm00317f

rsc.li/soft-matter-journal

1 Introduction

Aqueous solutions of surfactants exhibit rich lyotropic phase behaviour, arising from the self-assembly of amphiphilic molecules into a range of structures including micelles, liquid crystalline phases and crystalline solids, depending on composition, concentration and temperature.[1–5] These transitions define the physicochemical properties of the solution and underpin its functionality in formulated systems.[6–10] While boundaries between these states are often represented in equilibrium phase diagrams, the pathways between them can be strongly influenced by kinetic factors, particularly in concentrated systems where structural rearrangements are required.[3,11–14] As a result, the observed onset of ordering, and in particular crystallisation, may deviate significantly from equilibrium expectations, reflecting the interplay between thermodynamics and kinetics in complex self-assembled fluids.

Sodium dodecyl sulfate (SDS) is one of the most widely used anionic surfactants in formulated products, where it is typically employed at relatively high concentrations in the micellar regime to deliver cleaning and interfacial functionality.[15–19] However, aqueous SDS solutions are known to crystallise at temperatures close to ambient conditions within this concentration range (1–20 wt%), leading to loss of performance and challenges in storage stability.[14–18] The crystallisation behaviour of SDS has been shown to depend sensitively on experimental conditions, including cooling rate, sample volume and confinement, reflecting the strong influence of nucleation and growth kinetics on the observed crystallisation temperature.[19–21] As a result, reported phase boundaries for SDS systems may vary significantly depending on the measurement protocol, complicating the identification of equilibrium behaviour and limiting predictive control in practical formulations.

The addition of co-surfactants provides a potential route to modify the phase behaviour and crystallisation of SDS solutions, with amphoteric surfactants such as dimethyldodecylamine oxide (DDAO) known to reduce the critical micelle concentration, alter micellar structure and modify crystallisation behaviour.[17,21–23] Previous studies have reported a reduction in the apparent crystallisation temperature and changes in crystal morphology and growth kinetics upon addition of DDAO to SDS solutions.[21,23] However, these studies have largely focused on micellar systems,

[a] School of Mechanical Engineering, University of Leeds, Leeds, LS2 9JT, UK. E-mail: s.khodaparast@leeds.ac.uk
[b] School of Engineering, University of Liverpool, L69 3BX Liverpool, UK
[c] ISIS Pulsed Neutron and Muon Source, Science and Technology Facilities Council, Rutherford Appleton Laboratory, OX11 0QX Didcot, UK
[d] Chemical Engineering Department, Imperial College London, SW7 2AZ London, UK

with limited attention to the emergence of liquid crystalline phases at higher concentrations and their potential role in crystallisation. In addition, the reported crystallisation behaviour has primarily been assessed in terms of apparent crystallisation temperature, with limited consideration of the underlying kinetics and induction times associated with crystal formation. The formation of liquid crystalline phases introduces an intermediate state of orientational and positional order, within which crystallisation requires substantial structural rearrangement.[24] As a result, crystallisation pathways may differ fundamentally from those in isotropic micellar solutions, to extended induction times and strong sensitivity of the observed crystallisation onset to experimental protocol. Despite these implications, the coupling between liquid crystalline ordering and crystallisation kinetics in mixed surfactant systems remains largely unexplored.

Recent work has highlighted the strong coupling between anisotropic order and mechanical/structural arrest in surfactant-based lyotropic liquid crystalline systems, supporting the view that liquid-crystalline ordering can impose kinetic constraints on subsequent phase transformations.[24,25] To address the role of liquid crystalline ordering in surfactant crystallisation and its impact on observed phase behaviour, we investigate mixed SDS/DDAO systems at concentrations relevant to formulated applications. Using a combination of dynamic light scattering, cross-polarised optical microscopy and small-angle neutron scattering, we resolve the structural evolution of the system across micellar, liquid crystalline and crystalline regimes during controlled cooling. We identify the transition in composition at which liquid crystalline phases emerge and examine the temperature-concentration region in its vicinity, where crystallisation behaviour becomes strongly dependent on the underlying self-assembled structure. This approach enables direct comparison of crystallisation pathways originating from distinct phases and provides insight into the origin of delayed crystallisation in the presence of liquid crystalline order. The findings highlight the importance of pathway-dependent kinetics in determining the apparent crystallisation behaviour and the associated challenges in identifying equilibrium phase boundaries in complex surfactant systems.

2 Materials and methods

Sodium dodecyl sulfate, SDS (>99.0% purity) and an aqueous solution of 30 wt% DDAO were purchased from Sigma-Aldrich and used as received. Solutions for DLS and OM analyses were prepared by mixing the surfactants in deionised water. Homogeneous SDS solutions were doped with DDAO solution to achieve the desired concentration. Surfactant solutions for SANS measurements were prepared by mixing DDAO and SDS (both of >99.0% purity) in D_2O. Mole fractions of the surfactants were kept constant when substituting deionised water with D_2O.

2.1 Cross-polarised optical microscopy

CPOM was employed to detect phase transition from the isotropic micellar phase to the birefringent liquid crystalline and the crystalline phases, following procedures described in previous publications.[3,14] In summary, 3 μL of the solution was placed between two thin glass cover slips. Solvent evaporation during the experiments was minimised by sealing the area surrounding the droplet using a gasket. Isothermal experiments were performed by initially stabilising the droplet at 60 °C before a rapid quench (at 80 °C min^{-1}) to the final temperature of interest, using a Linkam THMS600 temperature control stage. OM images were captured with an Olympus BX41M-LED microscope, using a 10× objective and a CMOS camera (Basler ac2040-90) that provided an overall spatial resolution of 1.5 μm per pixel.

2.2 Dynamic light scattering (DLS)

DLS was performed using a Zetasizer Nano S (Malvern Panalytical), operating with a back-scattering detector (θ = 173°) and a 633 nm He–Ne laser. Samples were loaded in polystyrene cuvettes (pathlength 10 mm), with controlled temperature in the range of 60 °C down to 0 °C. Experiments were initiated at 60 °C to ensure isotropic micellar phase at the start of the measurements. The correlation data were interpreted for basic phase recognition without further fitting or analysis.

2.3 Small angle neutron scattering (SANS)

SANS experiments were performed under linear and quenching cycles on the Larmor diffractometer (ISIS, Harwell, UK), with a polychromatic λ = 0.9–13.3 Å unpolarised incident beam with sample-to-detector distance = 4.1 m, yielding a fixed momentum transfer range of approximately $0.005 < Q < 0.6$ $Å^{-1}$ with the peak flux in the intermediate Q range.[26] Fully dissolved surfactant solutions were loaded in quartz cells (1 mm banjo, Starna). All tests were started at 60 °C, where all solutions were in the isotropic micellar phase. Quiescent tests for phase mapping were performed by placing the quartz cells into a metallic sample changer that was thermally controlled using a liquid bath. Controlled cooling rates were applied using a Peltier devices to achieve nominal rates of 0.1 and 100 °C min^{-1}. The resulting SANS data were reduced, using standard procedures, in MANTID.[27]

3 Results

We focus on aqueous solutions containing 20 wt% SDS, a concentration of direct relevance to formulated systems where crystallisation occurs close to ambient conditions. Previous studies have shown that the addition of DDAO modifies the micellar structure through charge screening and promotes the formation of elongated aggregates even at low additive concentrations.[17,22,28,29] At higher DDAO contents, transitions to more ordered phases have been suggested, although their impact on crystallisation remains unclear.

3.1 Composition window

To identify the composition range of interest, we first examine the induction time for crystallisation in mixed SDS/DDAO solutions following rapid cooling to 4 °C. Importantly, the SDS concentration is held constant at 20 wt% across all compositions,

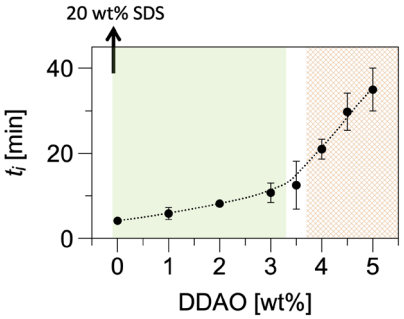

Fig. 1 Impact of DDAO incorporation on crystallisation induction time t_i of SDS solutions. The induction time is measured using DLS as a function of the wt% of added DDAO to an aqueous solution of 20 wt% SDS. Solutions with DDAO concentrations $\lesssim$3 wt% flow upon flipping the vial, while those at higher concentrations of DDAO appear as a gel with a significantly higher viscosity. The shaded regions highlight composition ranges exhibiting distinct crystallisation behaviour: the low-DDAO region corresponds to rapid crystallisation from a micellar phase, while the high-DDAO region corresponds to significantly delayed crystallisation associated with the formation of a liquid crystalline phase.

thus, any observed changes in crystallisation kinetics arise from modifications to self-assembled structure rather than variations in the total crystallising species. Fig. 1 shows the induction time, measured with DLS, defined as the time required for the first detectable crystalline structures to appear, as a function of DDAO concentration. For DDAO concentrations up to 3 wt%, the induction time increases gradually, remaining on the order of a few minutes. In contrast, a sharp increase in induction time is observed for DDAO concentrations $\geq$4 wt%, where crystallisation is delayed to several tens of minutes.

This marked change in behaviour identifies a transition between two distinct regimes of crystallisation kinetics, separated by a composition threshold between 3 and 5 wt% DDAO. Notably, this transition occurs without a corresponding shift in the crystallisation temperature, indicating that the observed delay is not primarily thermodynamic in origin. Instead, the abrupt increase in induction time suggests a change in the underlying self-assembled structure of the solution, motivating a detailed investigation of phase behaviour and crystallisation pathways within this composition window.

3.2 Phase behaviour

The phase behaviour of mixed SDS/DDAO solutions was characterised using DLS, CPOM and SANS, enabling identification of micellar (L_1), liquid crystalline (LC) and crystalline (C) phases across the temperature-composition space. Representative signatures of each phase are shown in Fig. 2.

The isotropic micellar phase (L_1), observed at lower DDAO concentrations and higher temperatures, is characterised by a rapidly decaying correlation function in DLS, the absence of birefringence in CPOM, and a broad structure factor peak in SANS corresponding to disordered micellar aggregates (Fig. 2c–e). In this regime, the addition of DDAO is known to promote growth and elongation of ellipsoidal micelles, resulting in increased solution viscosity compared to pure SDS systems.[17,22]

At higher DDAO concentrations, a transition to a gel-like self standing liquid crystalline phase is observed (Fig. 2a and b). This phase is identified by the appearance of birefringent textures in CPOM and the emergence of multiple peaks in the SANS profiles, consistent with a hexagonal arrangement of elongated cylindrical aggregates (Fig. 2c and e). The corresponding DLS correlation functions exhibit multiple decay modes, reflecting the presence of slow structural relaxation within the ordered phase (Fig. 2d). In particular, the liquid crystalline phase is detected at total surfactant concentrations as low as $\approx$25 wt% in mixed SDS/DDAO systems, significantly lower than those found for aqueous SDS solutions.[15,16,30–32]

Crystalline phases are identified by the appearance of strongly birefringent domains in CPOM and the emergence of a sharp Bragg peak at high Q in the SANS profiles, corresponding to the lamellar surfactant phase, consistent with SDS-rich structures (Fig. 2c). In DLS measurements, crystal formation is associated with the appearance of a slow decay mode at long correlation times (Fig. 2d).

The resulting phase diagram is summarised in Fig. 2b. The liquid crystalline phase occupies a composition range above approximately 3–4 wt% DDAO and spans a broad temperature window between the micellar and crystalline regions. Importantly, the emergence of the liquid crystalline phase coincides with the composition range over which a marked increase in crystallisation induction time was observed in Fig. 1. This correspondence indicates that the transition in crystallisation behaviour identified previously is associated with a change in the underlying self-assembled structure of the solution, from isotropic micelles to an ordered liquid crystalline phase.

The impact of the liquid crystalline phase on crystallisation behaviour is further illustrated by optical microscopy images obtained during isothermal tests at 4 °C (Fig. 3). For solutions containing $\lesssim$3 wt% DDAO, crystalline domains are observed within the isotropic micellar phase after relatively short times. In contrast, for DDAO concentrations $\geq$5 wt%, no crystalline structures are detected at early times despite the system being cooled below the crystallisation temperature. Instead, birefringent liquid crystalline textures persist, with crystal formation occurring only at later times as the liquid crystalline phase gradually disappears. These observations indicate that crystallisation is significantly delayed in the presence of liquid crystalline order.

3.3 Crystallisation pathways

The influence of liquid crystalline ordering on crystallisation is further examined by comparing the structural evolution of SDS/DDAO solutions across compositions spanning the two regimes identified in Fig. 1. Fig. 4 presents representative SANS profiles obtained during cooling for systems corresponding to pure SDS, intermediate DDAO content ($\lesssim$3 wt%), and compositions within the liquid crystalline regime ($\geq$5 wt%).

For pure SDS and low DDAO concentrations ($\lesssim$3 wt%), crystallisation proceeds directly from the isotropic micellar (left downward arrow in Fig. 2b). Upon cooling, the diffuse scattering associated with disordered micelles is progressively replaced by a sharp Bragg peak at high Q, indicating the formation of the

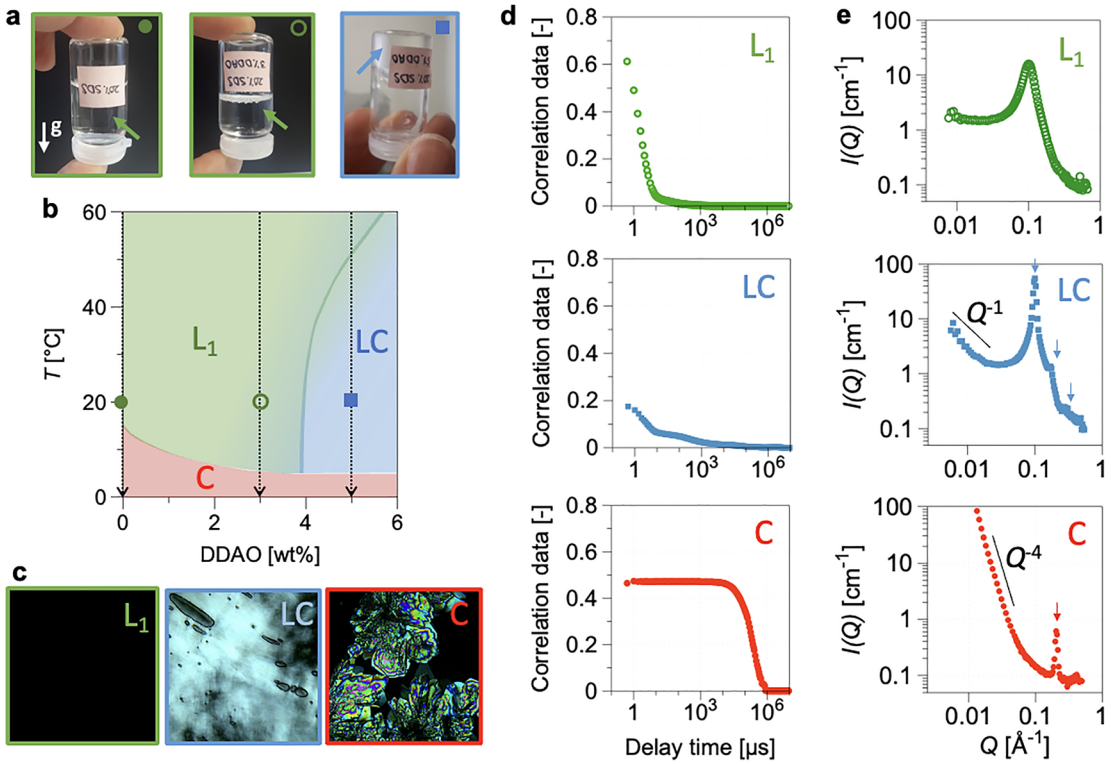

Fig. 2 Phase behaviour of aqueous solution of 20 wt% SDS with 0–6 wt% of added DDAO surfactant. The micellar/liquid crystal, micellar/crystalline and liquid crystal/crystalline phases indicate points where transition to the higher ordered phase is first detected. A combination of CPOM, DLS and SANS measurements is used to quantify the position of phase boundaries. Illustrated data in (a) and (c)–(d) correspond to temperature and concentrations identified on the phase diagram. Representative inverted vial macroscopic images of flowable micellar phases (left, 20 wt% SDS and middle, 20 wt% SDS + 3 wt% DDAO), and (right) self-standing gel-like liquid crystalline phase observed at ≥4–6 wt% DDAO. (b) Temperature-concentration phase map for a base solution of 20 w% SDS and varied DDAO content. (c) Example CPOM images representing the black micellar phase and birefringent liquid crystal and crystal phases. (d) Examples of DLS measurements showing a single high intensity fast decaying curve for the micellar phase (L_1, top), low intensity curve with multiple slower decaying functions for the liquid crystal phase (LC, middle) and longer delay time in the correlation function representing the formation of crystals within the solution (C, bottom). (e) Example SANS measurements of a broad peak at intermediate Q values representing the micellar phase (top), three peaks at Q, $\sqrt{3}Q$ and $\sqrt{7}Q$ corresponding to the hexagonal liquid crystal phase (middle) and a sharp Bragg peak demonstrating the bilayer structure of the surfactant crystals. Across a, b and c panels, L_1, LC and C refer to solutions of 20% SDS at 20 °C, 20% SDS + 3% DDAO at 20 °C and 20% SDS at 0 °C phases, respectively.

layered crystalline structure. No intermediate ordered phase is observed, and the transition occurs over relatively short timescales, consistent with the induction times reported in Section 3.1.

In contrast, for DDAO concentrations within the liquid crystalline regime (≥5 wt%), crystallisation follows a distinct pathway. Prior to the appearance of crystalline features, the system first forms a hexagonal liquid crystalline phase, characterised by multiple Bragg peaks at intermediate Q corresponding to the ordered arrangement of elongated cylindrical aggregates (right downward arrow in Fig. 2b). The subsequent emergence of crystalline peaks occurs only after prolonged times, indicating that crystallisation proceeds *via* transformation of the liquid crystalline phase rather than directly from the micellar state.

The comparison highlights a fundamental difference in crystallisation pathways across the composition range. While micellar systems undergo a direct transition from disordered aggregates to crystalline order, systems within the liquid crystalline regime follow a two-step pathway involving the formation of an intermediate ordered phase. This change in pathway is consistent with the marked increase in induction time observed at higher DDAO concentrations and suggests that the presence of liquid crystalline order introduces an additional structural barrier to crystallisation.

3.4 Time-resolved structural evolution

To further elucidate the origin of delayed crystallisation within the liquid crystalline regime, we examined the structural evolution of the 20 wt% SDS + 5 wt% DDAO system by SANS under both slow linear cooling (Fig. 5) and a rapid quench (Fig. 6) conditions. In particular, the evolution of the peak positions is quantitatively extracted and presented in Fig. 5b and Fig. 6c and d, allowing direct tracking of lattice spacing and structural changes within the hexagonal phase.

During linear cooling (Fig. 5a), the broad micellar scattering profile observed at 60 °C progressively transforms into that of a hexagonal liquid crystalline phase, marked by the emergence of the primary and second-order reflections with ratios consistent with 1 and $\sqrt{3}$. The third reflection becomes increasingly distinct at lower temperatures and approaches the $\sqrt{7}$ position as the structure becomes more ordered (Fig. 5b). After the

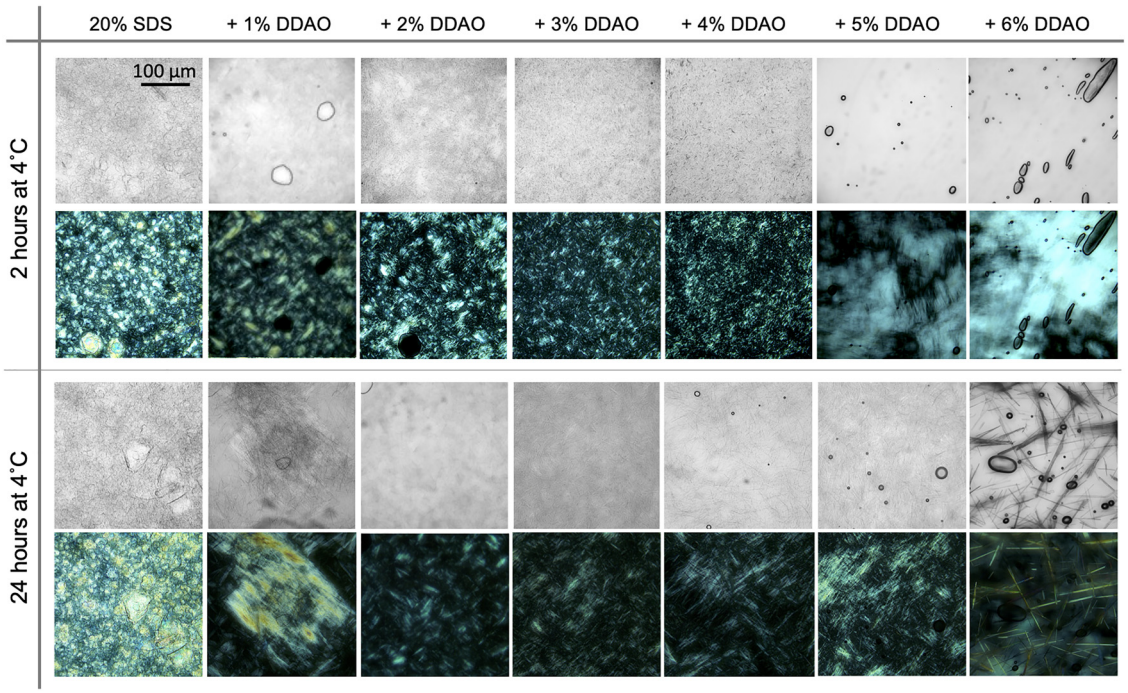

Fig. 3 Bright field (top row) and cross-polarised (bottom row) optical microscopy images of lamellar surfactant crystals in the mixed surfactant solutions of interest obtained in the bulk solution through cooling. 1–6 wt% DDAO was added to a base solution of 20 wt% SDS content. Mixed surfactant solutions were examined after 2 and 24 hours being held at 4 °C.

system reaches 0 °C, a second hexagonal population develops during the isothermal hold, giving rise to a transient splitting of the Bragg peaks. Over time, one of these populations gradually disappears, leaving a single hexagonal phase with larger spacing. In parallel, the low-Q scattering evolves from an approximately flat micellar profile ($\beta \approx 0$) to a slope close to -1, consistent with elongated cylindrical aggregates,[32] and finally approaches -4 as three-dimensional crystalline objects emerge.[33]

The corresponding evolution after rapid cooling from 60 to 0 °C is shown in Fig. 6. Immediately after quench, the system forms a hexagonal liquid crystalline phase, which is retained for an extended period before clear crystalline signatures appear. As in the slowly cooled sample, the hexagonal phase subsequently divides into two populations and later converges to a single phase at larger spacing before the appearance of the crystal bilayer Bragg peak (Fig. 6a and b). During this process, the shift of the primary peak to lower Q corresponds to an increase in lattice spacing within the hexagonal phase. This evolution, quantified in Fig. 5b and 6c, d, indicates progressive structural rearrangement of the cylindrical aggregates during cooling and isothermal holding. The transient coexistence of two hexagonal populations, identified by distinct peak positions, indicates the presence of domains with different lattice spacings. This behaviour is consistent with an evolving internal structure within the liquid crystalline phase rather than a static mesophase. In contrast to the gradual ordering observed during slow cooling, the quench test measurements resolve the delayed induction of crystallisation at a fixed temperature. Throughout this structural transformation, the three reflections retain the ratios $1:\sqrt{3}:\sqrt{7}$ (Fig. 6d), confirming that the system retains hexagonal symmetry, indicating that crystallisation proceeds *via* transformation within an ordered phase rather than from a disordered state. The low-Q exponent follows the same sequence observed under slow cooling, changing from approximately 0 in the isotropic micellar state to around -1 upon formation of long hexagonally packed cylindrical aggregates and then to -4 as three-dimensional crystals appear, providing a continuous structural signature of the transformation pathway (Fig. 6e).

The CPOM images and schematics in Fig. 6b provide a complementary real-space description of this pathway. The structural evolution proposed in this panel is consistent with the temperature-dependent micellar growth previously reported for SDS/DDAO mixtures, in which initially ellipsoidal micelles become increasingly elongated on cooling. In the present system, the emergence of sharp Bragg reflections and a low-Q exponent close to -1 indicates the formation of finite cylindrical aggregates that subsequently organise into a hexagonal liquid crystalline phase. The relatively tight packing observed in this regime suggests that the cylinders retain an anisotropic, likely tilted ellipsoidal cross-section. Further cooling is accompanied by a shift of the primary peak to lower Q, consistent with continued aggregate growth and increasing characteristic spacing within the ordered phase. The appearance of two coexisting hexagonal populations at later times suggests the emergence of a secondary ordered structure during the approach to crystallisation. Notably, this second population develops concurrently with the appearance of the bilayer Bragg peak associated with lamellar crystalline phase. This behaviour is consistent with a structural rearrangement in which the elongated cylindrical

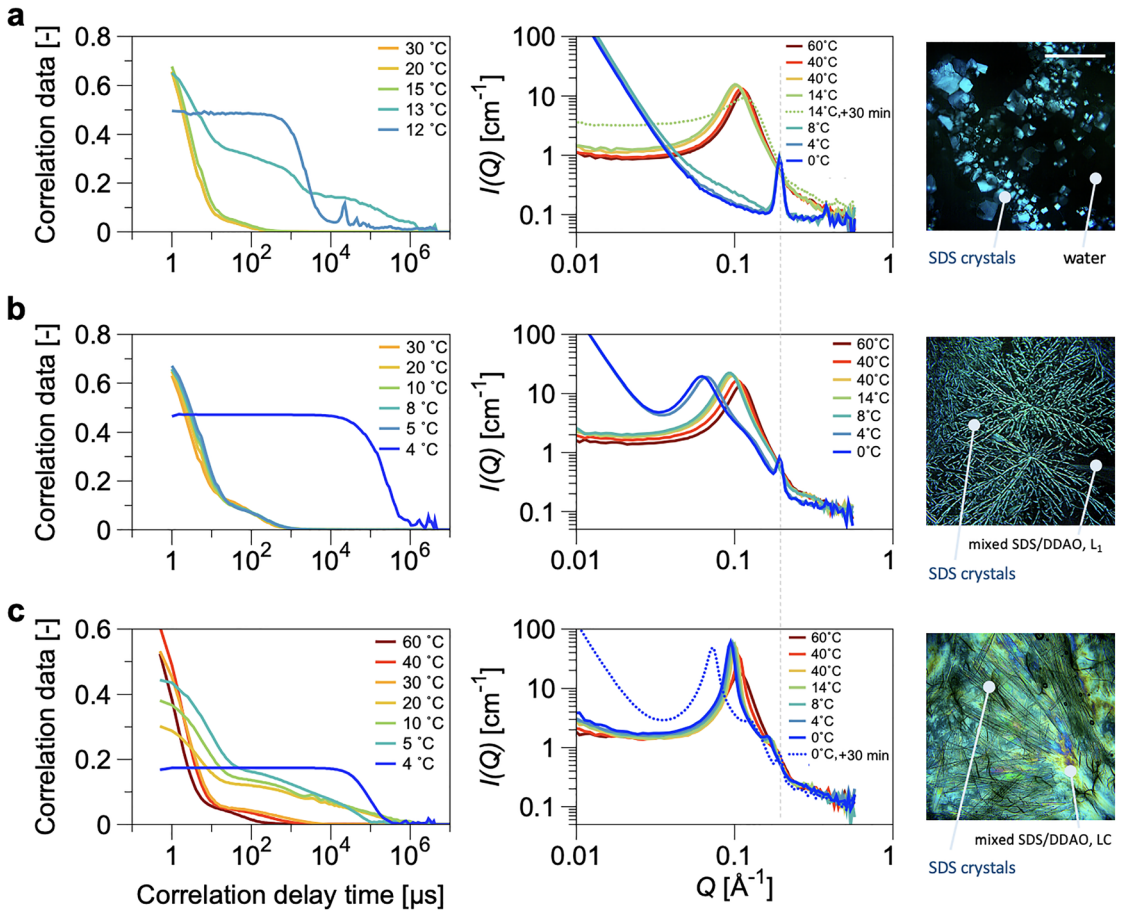

Fig. 4 Transformation pathways of crystal formation from the micellar surfactant solutions demonstrated by DLS and SANS data for (a) 20 wt% SDS, (b) 20 + 3 wt% SDS/DDAO and (c) 20 + 5 wt% SDS/DDAO. Average cooling rate in all experiments is 0.1 °C min^{-1}. SANS data after isothermal wait time (+30 min) is included close to the phase boundaries. The CPOM images on the right show lamellar crystalline phase within (a) water, (b) micellar solution and (c) birefringent hexagonal solution at 0 °C. Scale bar corresponds to 100 μm in all images.

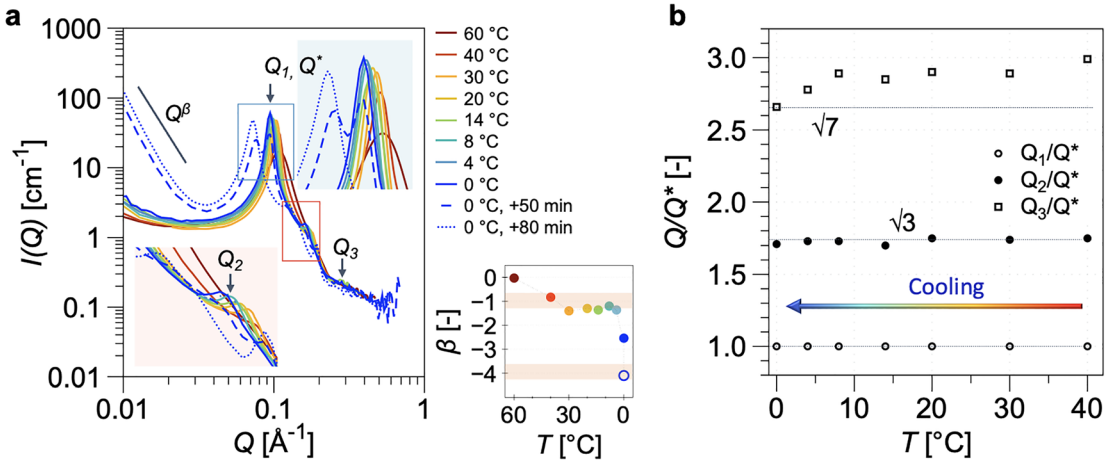

Fig. 5 SANS data for mixed 20 + 5 wt% SDS/DDAO during a linear cooling cycles at 0.1 °C min^{-1} with pauses for data acquisition at different temperatures. (a) Intensity *versus* scattering vector graph shows transformation from the broader central peak of the micellar solution at 60 °C to the hexagonal liquid crystal phase identified based on the appearance of the 1 : $\sqrt{3}$ lattice peaks. No clear indication of crystal formation is observed when cooling the solution 0 °C. A secondary hexagonal population was observed for the sample kept at 0 °C, whose development and growth consumed the first population after around 80 min of wait time at 0 °C. Inset graph refers to the power of fit to the low-Q region demonstrating the transition from 0 (micellar phase) to −1 (hexagonally packed elongated cylinders) at intermediate temperatures and finally to −4 (three-dimensional crystal aggregates) at later times at 0 °C. (b) The ratio the magnitude of Q at the second and third peak to Q_1.

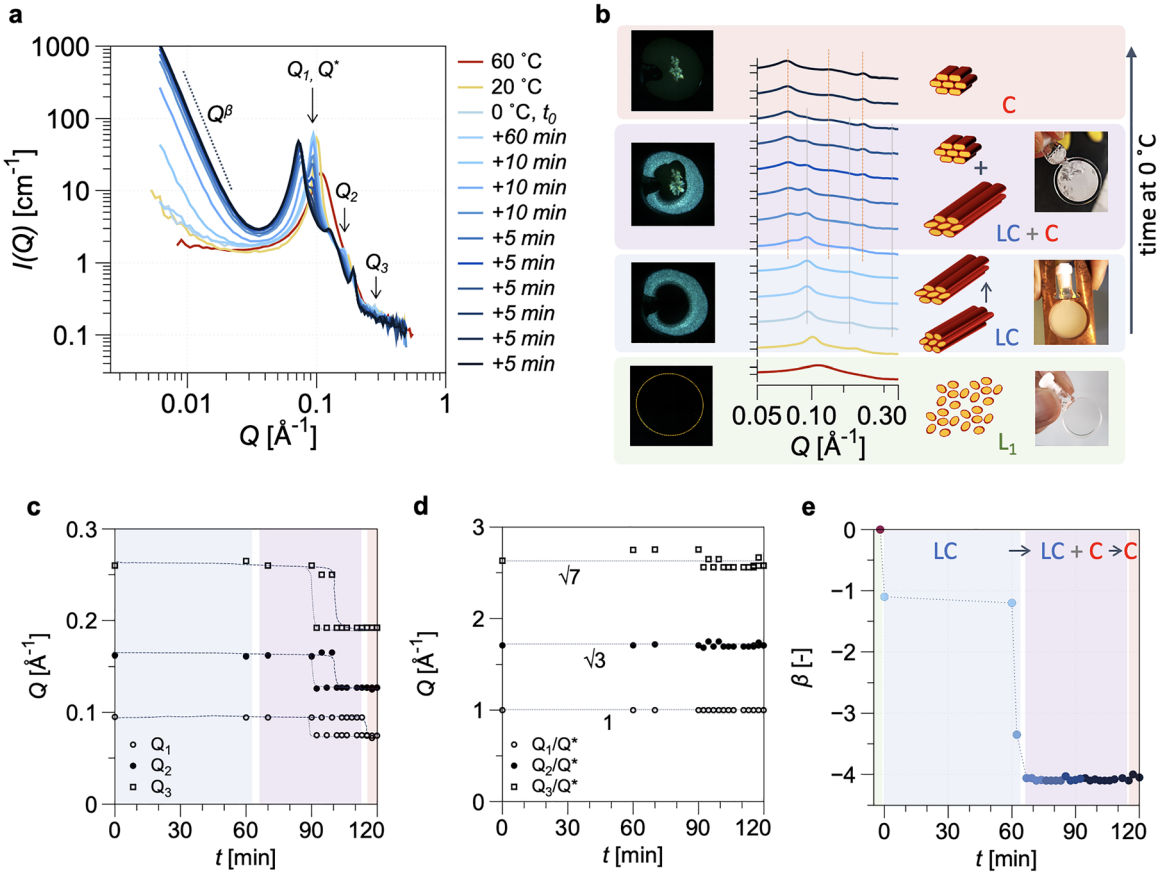

Fig. 6 Crystallisation within the liquid crystal solution of 20 + 5 wt% SDS/DDAO collected during quenching experiments. (a) SANS data for the rapidly cooled solution at 100 °C min^{-1} from 60 °C and kept at 0 °C. SANS data collected at 60 °C and 20 °C are included in the graph for reference. The hexagonal liquid crystal phase is identified by the appearance of the $1:\sqrt{3}:\sqrt{7}$ lattice order peaks labeled as Q_1, Q^*, Q_2 and Q_3. A power law fit Q^{β} represents the behaviour of the I–Q curve in the low-Q region. (b) Temporal SANS data of the triple hexagonal peak taken from (a) with time evolving from bottom to top. Inset images on the left show CPOM (300 × 300 μm^2 region) of a droplet of the mixed 20 + 5 wt% SDS/DDAO cooled from the bottom and kept at 0 °C. Schematics show the transformation from ellipsoidal micelles to hexagonal packed cylinders of ellipsoidal cross-sections (LC) and later to the co-existing hexagonal liquid crystalline and templated crystalline phase (LC + C) before evolving into a fully lamellar crystal structure in with a hexagonal order. Images on the right show examples of the micellar, liquid crystalline and mixed LC + C phase samples in SANS sampling cuvette. (c) and (d) Absolute and relative Q values of the peak positions, showing hexagonal order across the tested temperatures. (e) Slope of the power-law fit to the low-Q regions shows transition from isotropic micelles (β = 0) to elongated one-dimensional cylinders (β = −1) to three-dimensional crystals (β = −4).

aggregates progressively flatten into ribbon-like bilayer objects while partially retaining hexagonal positional order. Such an intermediate state would provide a plausible structural pathway between the hexagonal mesophase and the final lamellar crystal structure, and may explain the prolonged coexistence of liquid crystalline and crystalline features observed during the transformation.

These observations show that crystallisation in the liquid crystalline regime does not proceed directly from the micellar state, but *via* a delayed transformation of a hexagonally ordered mesophase. This intermediate phase therefore acts as a kinetically hindered state, within which structural reorganisation is required before the final lamellar crystal structure can form. More broadly, the presence of a liquid crystalline phase fundamentally alters the relationship between crystallisation temperature and structural state. Although crystallisation ultimately occurs at similar temperatures across the composition range, the pathway and timescale of the transformation depend strongly on whether the system is in a micellar or liquid crystalline state. In the latter case, the ordered mesophase introduces an additional structural constraint with associated energetic barriers, requiring reorganisation of elongated aggregates prior to crystal formation. The increase in lattice spacing and coexistence of domains suggest a gradual transformation of the aggregate morphology toward structures compatible with lamellar crystalline order. While the precise nature of this rearrangement cannot be uniquely determined from small-angle scattering alone, it likely involves significant re-organisation of surfactant packing within the liquid crystalline phase. As a result, the observed crystallisation temperature no longer reflects a direct thermodynamic phase boundary, but rather the interplay between phase behaviour and kinetic accessibility. This behaviour highlights the difficulty in identifying equilibrium crystallisation boundaries in the vicinity of liquid crystalline phases, where experimentally observed transitions are strongly influenced by kinetic limitations.

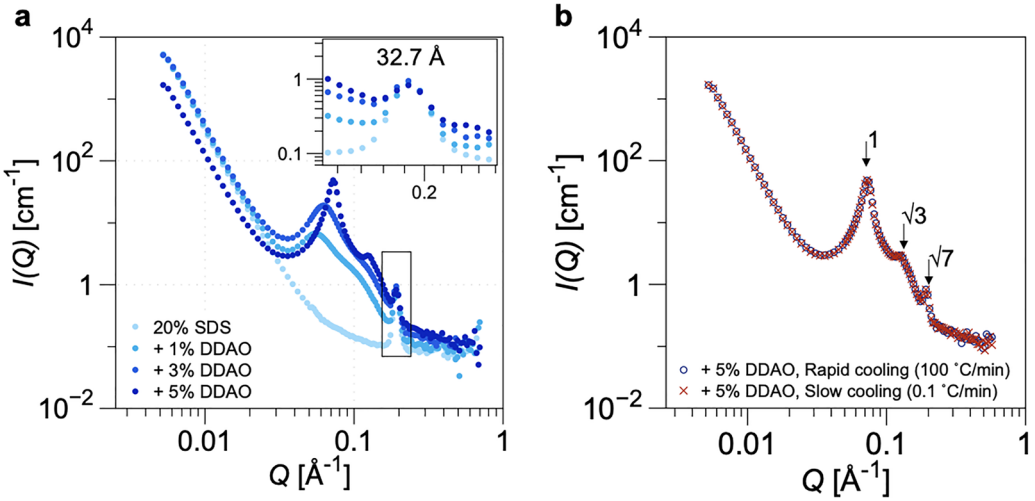

Fig. 7 Small-angle neutron scattering (SANS) profiles of mixed SDS/DDAO systems illustrating the structure of the liquid crystalline phase and its robustness to thermal history. (a) Scattering intensity profiles for 20 wt% SDS with varying DDAO concentrations (0–5 wt%), showing the evolution from micellar scattering to the emergence of pronounced Bragg peaks at intermediate Q corresponding to the formation of an ordered liquid crystalline phase. The inset highlights the primary peak position, indicating a characteristic spacing of approximately 32.7 Å. (b) Comparison of SANS profiles for a system containing 5 wt% DDAO obtained under quenching and linear cooling conditions. The positions of the Bragg peaks follow the ratios $1:\sqrt{3}:\sqrt{7}$ consistent with a hexagonal arrangement of cylindrical aggregates. The agreement between cooling protocols indicates that the structure of the liquid crystalline phase is independent of thermal history.

The structural characteristics of the crystalline phase are further examined in Fig. 7. The SANS profiles in Fig. 7a show that the position of the high-Q Bragg peak associated with the SDS bilayer remains unchanged upon addition of DDAO, corresponding to a characteristic spacing of approximately 32.7 Å across all compositions studied. This indicates that the internal structure of the crystals is not significantly altered by the presence of the co-surfactant.[14] Comparison with reported crystallographic data shows that this spacing lies between those of highly hydrated (mono- and hemihydrate) and low-hydration (1/8 hydrate and anhydrous) SDS crystal structures, suggesting a hydrated lamellar phase with possible contributions from less hydrated packing motifs.[34] As the present measurements are limited to small-angle scattering, which probes only the lamellar repeat distance, we do not assign a specific hydrate, polymorph, or crystal composition. In particular, we cannot exclude partial incorporation of DDAO or the formation of mixed surfactant crystalline phases. A definitive structural and compositional identification would require wide-angle diffraction or spatially resolved spectroscopic measurements, which are not included in the present study. Fig. 7b compares the final structures obtained following isothermal crystallisation at 0 °C and linear cooling. The scattering profiles overlap closely, with Bragg peak positions following the ratios $1:\sqrt{3}:\sqrt{7}$, demonstrating that the same hexagonally structured bilayer crystalline phase is formed under both conditions. These observations indicate that the final crystalline structure is independent of both composition and cooling pathway. The delayed crystallisation observed in the presence of liquid crystalline phases does not thus arise from differences in the final crystal structure, but rather from kinetic constraints associated with the transformation pathway leading to this equilibrium state.

4 Conclusions

The phase behaviour and crystallisation of mixed SDS/DDAO surfactant systems were investigated using a combination of scattering and microscopy techniques, enabling direct correlation between nanoscale structure and macroscopic crystallisation behaviour. The addition of DDAO was found to promote the formation of a hexagonal liquid crystalline phase at concentrations significantly lower than in pure SDS systems, introducing a distinct regime of self-assembly at compositions relevant to formulated applications.

Within this regime, crystallisation is markedly delayed, with induction times increasing by orders of magnitude despite only minor changes in the apparent crystallisation temperature. Structural analysis demonstrates that this delay arises from a change in crystallisation pathway, with systems transitioning from direct crystallisation of micellar solutions to a two-step process involving the formation and subsequent transformation of a liquid crystalline phase. This intermediate ordered state imposes constraints on molecular rearrangement, resulting in kinetically hindered crystallisation.

These findings highlight that, in the vicinity of liquid crystalline phase boundaries, the experimentally observed crystallisation behaviour is strongly governed by kinetics rather than equilibrium thermodynamics. As a result, apparent phase boundaries may be highly dependent on experimental protocol and timescale. The results provide a framework for understanding and controlling crystallisation in mixed surfactant systems and are expected to be relevant to a broad range of formulations in which mesophase formation precedes crystallisation. More broadly, these results demonstrate that the presence of intermediate mesophases can decouple crystallisation kinetics from equilibrium

thermodynamics, with important implications for the interpretation of phase diagrams in complex self-assembled systems.

Conflicts of interest

There are no conflicts to declare.

Data availability

The data that support the findings of this study are available from the corresponding author upon reasonable request. SANS data is available here: DOI: https://doi.org/10.5286/ISIS.E.RB1820374[26].

Acknowledgements

Experiments at the ISIS Neutron and Muon Source were supported by beamtime allocation RB1820374 from the Science and Technology Facilities Council.

References

1 R. G. Laughlin, *The aqueous phase behavior of surfactants*, Academic Press, 1996.
2 J. Liu, L. Guan and Z. Wang, *Colloids Surf., A*, 2020, **585**, 124019.
3 S. Khodaparast, W. Sharratt, H. Wang, E. S. Robles, R. Dalgliesh and J. T. Cabral, *J. Colloid Interface Sci.*, 2019, **546**, 221–230.
4 G. Tiddy, *Phys. Rep.*, 1980, **57**, 1–46.
5 G. A. Ferreira, *J. Dispersion Sci. Technol.*, 2022, **43**, 2165–2178.
6 T. Engels and W. von Rybinski, *J. Mater. Chem.*, 1998, **8**, 1313–1320.
7 M. J. L. Castro, C. Ojeda and A. F. Cirelli, Surfactants in Agriculture. In Green Materials for Energy, Products and Depollution, *Environmental Chemistry for a Sustainable World*, Springer, Dordrecht, 2013, vol. 3.
8 J. Falbe, *Surfactants in consumer products*, Springer, 1987.
9 J. J. Scheibel, *J. Surfactants Deterg.*, 2004, **7**, 319–328.
10 S. Fuller, Y. Li, G. J. T. Tiddy, E. Wyn-Jones and R. D. Arnell, *Langmuir*, 1995, **11**, 1980–1983.
11 W. A. Tiller, *The Science of Crystallization: Microscopic Interfacial Phenomena*, Cambridge University Press, Cambridge, 1991.
12 J. Leng, S. U. Egelhaaf and M. E. Cates, *Biophys. J.*, 2003, **85**, 1624–1646.
13 T. M. Weiss, T. Narayanan, C. Wolf, M. Gradzielski, P. Panine, S. Finet and W. I. Helsby, *Phys. Rev. Lett.*, 2005, **94**, 038303.
14 S. Khodaparast, J. Marcos, W. N. Sharratt, G. Tyagi and J. T. Cabral, *Langmuir*, 2021, **37**, 230–239.
15 P. Kékicheff, C. Grabielle-Madelmont and M. Ollivon, *J. Colloid Interf. Sci.*, 1989, **131**, 112–132.
16 P. Kékicheff, *J. Colloid Interface Sci.*, 1989, **131**, 133–152.
17 S. Khodaparast, W. N. Sharratt, G. Tyagi, R. M. Dalgliesh, E. S. Robles and J. T. Cabral, *J. Colloid Interface Sci.*, 2021, **582**, 1116–1127.
18 E. Summerton, G. Zimbitas, M. Britton and S. Bakalis, *Trends Food Sci. Technol.*, 2017, **60**, 23–30.
19 R. M. Miller, O. Ces, N. J. Brooks, E. S. J. Robles and J. T. Cabral, *Cryst. Growth Des.*, 2017, **17**, 2428–2437.
20 R. M. Miller, J. T. Cabral, E. S. J. Robles, N. J. Brooks and O. Ces, *CrystEngComm*, 2018, **20**, 6834–6843.
21 E. Summerton, M. J. Hollamby, G. Zimbitas, T. Snow, A. J. Smith, J. Sommertune, J. Bettiol, C. Jones, M. M. Britton and S. Bakalis, *J. Colloid Interface Sci.*, 2018, **527**, 260–266.
22 G. Tyagi, D. Seddon, S. Khodaparast, W. N. Sharratt, E. S. Robles and J. T. Cabral, *Colloids Surf., A*, 2021, **618**, 126414.
23 E. Summerton, G. Zimbitas, M. Britton and S. Bakalis, *J. Cryst. Growth*, 2016, **455**, 111–116.
24 C. D. Syme, J. Mosses, M. González-Jiménez, O. Shebanova, F. Walton and K. Wynne, *Sci. Rep.*, 2017, **7**, 42439.
25 K. Steck, S. Dieterich, C. Stubenrauch and F. Giesselmann, *J. Mater. Chem. C*, 2020, **8**, 5335–5348.
26 S. Khodaparast, W. N. Sharratt, R. M. Dalgleish and J. T. Cabral, *STFC ISIS Neutron and Muon Source*, 2018, DOI: 10.5286/ISIS.E.RB1820374.
27 O. Arnold, J. C. Bilheux, J. M. Borreguero, A. Buts, S. I. Campbell, L. Chapon, M. Doucet, N. Draper, R. Ferraz Leal, M. A. Gigg, V. E. Lynch, A. Markvardsen, D. J. Mikkelson, R. L. Mikkelson, R. Miller, K. Palmen, P. Parker, G. Passos, T. G. Perring, P. F. Peterson, S. Ren, M. A. Reuter, A. T. Savici, J. W. Taylor, R. J. Taylor, R. Tolchenov, W. Zhou and J. Zikovsky, *Nucl. Instrum. Methods Phys. Res., Sect. A*, 2014, **764**, 156–166.
28 L. M. G. Torquato, G. Tyagi, W. N. Sharratt, Z. Ahmad, N. Mahmoudi, J. Gummel, E. S. J. Robles and J. T. Cabral, *Langmuir*, 2024, **40**, 7433–7443.
29 L. M. G. Torquato, G. Tyagi, Z. Ahmad, L. Donina, N. Mahmoudi, R. Fong, P. F. Luckham and J. T. Cabral, *Soft Matter*, 2025, **21**, 5494–5502.
30 P. Kékicheff and B. Cabane, *Acta Crystallogr., Sect. B: Struct. Sci.*, 1988, **44**, 395–406.
31 M. Choudhary and S. M. Kamil, *ACS Omega*, 2020, **5**, 22891–22900.
32 R. Itri and L. Q. Amaral, *J. Phys. Chem.*, 1990, **94**, 2198–2202.
33 M. J. Hollamby, *Phys. Chem. Chem. Phys.*, 2013, **15**, 10566–10579.
34 L. Smith, A. Duncan, G. Thomson, K. Roberts, D. Machin and G. McLeod, *J. Cryst. Growth*, 2004, **263**, 480–490.